Chapter 2
New Heusler Compounds and Their Properties

Benjamin Balke, Gerhard H. Fecher, and Claudia Felser

Abstract Spintronics is a multidisciplinary field and a new research area. New materials must be found for satisfying the different types of requirement. The search for stable half-metallic ferromagnets and ferromagnetic semiconductors with Curie temperatures higher than room temperature is still a challenge for solid state scientists. A general understanding of how structures are related to properties is a necessary prerequisite for material design. Computational simulations are an important tool for a rational design of new materials. The new developments in this new field are reported from the point of view of material scientists.

2.1 Introduction

A great scientific interest is attracted by materials with a complete spin polarization at the Fermi energy [1]. Such materials, being a metal for spin up and a semiconductor (or insulator) for spin down electrons, are called half-metallic ferromagnets (HMF) [2, 3]. Already in 1983 Heusler compounds have been considered potential candidates to show this property. Theoretical calculations predicted an energy gap for minority electrons for the half-Heusler compound NiMnSb [2, 4] which, however, has been controversially discussed later [5–7]. At the same time, Kübler et al. [8] recognized that the minority spin densities at the Fermi energy (ε_F) nearly vanish for Co_2MnAl and Co_2MnSn. The authors concluded that this should lead to

B. Balke · G.H. Fecher · C. Felser
Institut für Anorganische Chemie und Analytische Chemie, Johannes Gutenberg – Universität, 55099 Mainz, Germany

B. Balke
e-mail: balke@uni-mainz.de

G.H. Fecher · C. Felser (✉)
Max-Planck-Institut für Chemische Physik fester Stoffe, 01187 Dresden, Germany
e-mail: felser@cpfs.mpg.de

G.H. Fecher
e-mail: fecher@cpfs.mpg.de

C. Felser, G.H. Fecher (eds.), *Spintronics*, DOI 10.1007/978-90-481-3832-6_2,

peculiar transport properties in these Heusler compounds because only the majority density contributes to the states at ε_F.

Generally, Heusler compounds belong to a group of ternary intermetallics with the stoichiometric composition X_2YZ ordered in an $L2_1$-type structure. Many of them are ferromagnetic [9]. X and Y are transition metals and Z is usually a main group element. Y may also be replaced by a rare earth element. The $L2_1$ structure consists of a primitive *fcc* lattice with a basis of four atoms. Remarkably, the prototype Cu_2MnAl is a ferromagnet even though none of its constituents is one [10].

The quite new research area of so-called *spintronics* is a multidisciplinary field. New materials must be found for satisfying the different types of requirement. The search for stable half-metallic ferromagnets and ferromagnetic semiconductors with Curie temperatures higher than room temperature is still a challenge for solid state scientists. A general understanding of how structures are related to properties is a necessary prerequisite for material design. Computational simulations are an important tool for a rational design of new materials. The new developments in this new field are reported from the point of view of material scientists. The development of magnetic Heusler compounds specifically designed as material for spintronics applications made tremendous progress in the very recent past.

The boom about Heusler compounds for spintronics applications and with it the huge number of both, theoretical and experimental investigations (over 700 publications concerning X_2YZ Heusler compounds in the last eight–nine years) began in 2002/2003 with the observation of—at that time—large negative magnetoresistance in powder compacts of $Co_2Cr_{0.6}Fe_{0.4}Al$ [11]. A magnetoresistive effect of 30 % in a small magnetic field of 0.1 T at room temperature was found. This demonstrated for the first time the feasibility of a cheap and simple magnetic sensor based on polycrystalline, intermetallic materials. This value was later optimized by using powder compacts of $Co_2Cr_{0.6}Fe_{0.4}Al$, mixed with insulating Al_2O_3, to a maximum magnetoresistance ratio of 88 % in an induction field of 0.125 T at 295 K [12].

Based on band structure calculations and guided by striking features in the electronic structure of several magnetic Heusler compounds, $Co_2Cr_{0.6}Fe_{0.4}Al$ was chosen to obtain a half-metallic ferromagnet with a van Hove singularity in the vicinity of the Fermi energy in the majority spin channel and a gap in the minority spin channel [11]. Following this investigation, Inomata et al. [13] prepared a spin valve type tunneling junction with a $Co_2Cr_{0.6}Fe_{0.4}Al$ Heusler compound film that showed a tunneling magnetoresistance ratio of 16 % at room temperature. Afterwards, thin films of the compound $Co_2Cr_{0.6}Fe_{0.4}Al$ were successfully grown by many other groups [14–17]. A magnetoresistance ratio of 26.5 % [13] (at 5 K) and 19 % [18] (at room temperature) was found for a tunneling magnetoresistance (TMR) element of the same compound. Very recently, Marukame et al. [19] reported a TMR ratio of 74 % at 55 K for a $Co_2Cr_{0.6}Fe_{0.4}Al$-MgO-CoFe magnetic tunnel junction. A spin polarization of only less than 49 % was found for polycrystalline samples by means of Andreev reflections [20]. The observation of an incomplete spin polarization may not only be caused by the model used to interpret the data [20, 21] but also by the properties of the sample. Clifford et al. [22] reported a spin polarization of 81 % in point contacts of $Co_2Cr_{0.6}Fe_{0.4}Al$.

However, the TMR ratios found in tunneling experiments indicate a spin polarization that is still too low, and not only at room temperature. This work reports on the investigation of the reasons of this contradiction between theory and experiment and with this knowledge it was tried to overcome the problems by designing new materials suitable for spintronics applications.

2.2 Experimental Details

Polycrystalline ingots of the compounds were prepared by arc melting of stoichiometric amounts of high purity elements in an argon atmosphere to avoid oxygen contamination at a pressure of 10^{-4} mbar. Additionally, a Ti sponge was used to bind remaining oxygen. The samples were melted three times. They were turned over after each melting process to yield a homogeneous sample. The weight loss after the whole melting procedure was less than 1 %. The polycrystalline ingots were annealed in evacuated quartz tubes at 1073 K for two weeks. The crystallographic structure was investigated by X-ray powder diffraction (XRD) using excitation by Mo–K_α radiation ($\lambda = 0.7093165$ nm; Bruker, AXS D8) in reflection geometry. The experimental diffraction patterns were refined using the FULLPROF program [23]. Additional synchrotron-based anomalous XRD investigations were carried out for various samples, due to the restrictions of powder XRD using laboratory source. The anomalous XRD experiments and the temperature dependent XRD measurements were performed at the X-ray powder diffraction beamline at the bending magnet $D10$ at the Brazilian Synchrotron Light Laboratory (LNLS). For details about the characteristics of the beamline see [24]. A scanning electron microscope (SEM, Jeol JSM-6400) equipped with an energy dispersive X-ray spectroscopy (EDX) detection system (EUMEX EDX) was used to check the homogeneity and stoichiometry of the samples. The measurements were carried out at a pressure of 3×10^{-6} mbar. An acceleration voltage of 20 kV was applied and an inspection angle of 35° was set up. For the correction of the quantitative data the ZAF method was applied which relies on atomic number (Z), absorption (A) and fluorescence (F) effects. The images were acquired via the Digital Image Processing System (DIPS) and the quantitative chemical analysis was performed with the program WINEDS 4.0. Magneto-structural investigations were carried out by Mößbauer spectroscopy in transmission geometry using a constant acceleration spectrometer. For excitation, a ^{57}Co(Rh) source with a line width of 0.105 mm/s and a $Ca^{119}SnO_3$ source with a line width of 0.3 mm/s was used in the case of Fe and Sn, respectively. The spectra of powder samples were measured at 290 K. The magnetic properties were investigated by a superconducting quantum interference device (SQUID, Quantum Design MPMS-XL-5) using nearly punctual pieces of approximately 5 mg to 10 mg of the sample. The measurements of the Seebeck coefficient were carried out with a Physical Property Measurement System (Model 6000 Quantum Design) on bars of about $(2 \times 2 \times 8)$ mm^3 which were cut from the pellets and polished before the measurement. In the temperature range above 350 K the Seebeck coefficient was

measured by a steady-state method using the RZ2001i measurement system from Ozawa science, Japan. For more details about the preparation, structural and magnetic properties see [25–28].

2.3 Crystal Structures of Heusler Compounds

In general, Heusler compounds crystallize in the Cu_2MnAl-type structure but in many cases certain types of disorder are observed. For a detailed description of the crystal structure as well as different types of atomic disorder see the contribution "*Crystal Structure of Heusler compounds*" by Tanja Graf and Claudia Felser. The relationship of the chemical ordering and the spin polarization is discussed there and useful experimental methods for the structural analysis of Heusler compounds are presented there.

2.4 Optimization of Co_2YZ Heusler Compounds

2.4.1 Investigation on $Co_2Cr_{0.6}Fe_{0.4}Al$

To understand why the spin polarization is too low, the structural and physical properties of the series $Co_2Cr_{1-x}Fe_xAl$, with varying iron concentration x, were investigated in detail. The results from X-ray diffraction (XRD) as well as an extended X-ray absorption fine structure (EXAFS) analysis and ^{57}Fe Mößbauer spectroscopy indicated structures in the bulk of the compound $Co_2Cr_{1-x}Fe_xAl$ that were different from those at the surface of the compound [29–31].

Figure 2.1 displays the EXAFS results for $Co_2Cr_{0.6}Fe_{0.4}Al$ and compares powder (higher amount of surface contribution) with bulk samples. The differences are clearly visible. The results corroborate those found from variable incidence XRD measurements, and indicate that the surface shows no ordered structure ($A2$-type) while the bulk is $B2$-like disordered. Indeed, the spectra provide no indication of the $L2_1$ structure, and this explains the reduced spin polarization.

Mößbauer spectroscopy was used to further explore the magneto-structural properties of $Co_2Cr_{0.6}Fe_{0.4}Al$. The results of both transmission and conversion electron Mößbauer spectroscopy (CEMS) were analyzed to obtain insight into both the disorder effects as well as the differences between the bulk and surface properties. It was found that rough mechanical treatment of the surfaces of bulk samples induces strong dynamic or relaxation effects. From the CEMS analysis, it was found that one of the best procedures for cleaning the surface of $Co_2Cr_{0.6}Fe_{0.4}Al$ was achieved by using grazing incidence Ar^+ ion bombardment (this was also checked for other compounds that are not shown here). Figure 2.2 shows the CEMS spectrum of ^{57}Fe enriched $Co_2Cr_{0.6}Fe_{0.4}Al$ bulk material after polishing followed by 60 min of Ar^+ ion bombardment in an UHV chamber. Even without any post-annealing for healing

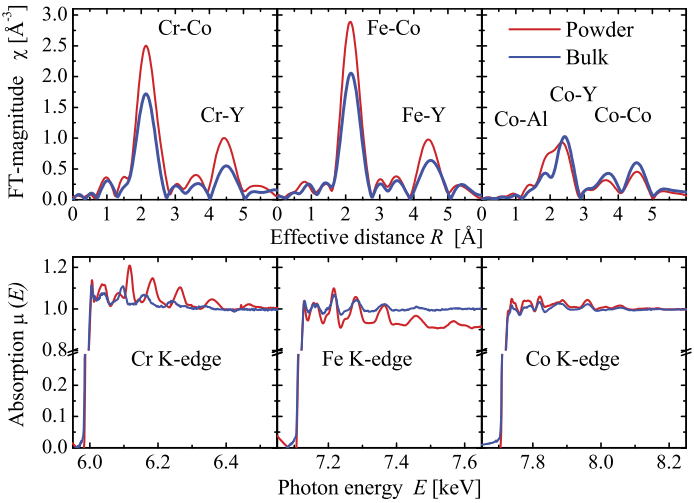

Fig. 2.1 EXAFS results of $Co_2Cr_{0.6}Fe_{0.4}Al$ comparing powder and bulk. Spectra taken at the Cr, Fe, and Co K-edges are compared for powder and bulk samples

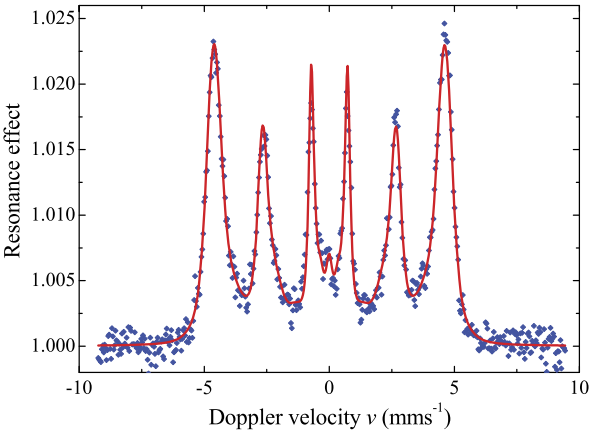

Fig. 2.2 CEMS spectrum of ^{57}Fe enriched $Co_2Cr_{0.6}Fe_{0.4}Al$ bulk material after 60 min Ar^+ ion bombardment

the surface, the spectra reveal the bulk magnetic properties as found in comparison to transmission Mößbauer experiments (please, note that, as reported in the chapter about photoemission experiments), the information depth of CEMS is comparable to that of high energy photoemission.

The studies of $Co_2Cr_{0.6}Fe_{0.4}Al$ were followed by a comprehensive characterization of other Cr-containing Heusler compounds. This is necessary for understanding the mechanism that causes a magnetic moment of Cr in that compound that is less than that found in the isoelectronic $Co_2Cr_{1-x}Fe_xGa$ compounds. Co_2CrZ Heusler compounds (Z = Al, Ga) are already known; the next compound with an element from the series of main group elements is the Co_2CrZ Heusler compound with

Z = In. This compound had not been reported before, so Co_2CrIn was synthesized and characterized [32]. In summary, this compound is $L2_1$ ordered and exhibits no antisite disorder. Co_2CrIn was found to be a ferrimagnet with a magnetic moment of 1.18 μ_B at 5 K. In addition, the hysteresis indicates a soft magnetic behavior. The value of the measured magnetic moment is not an integer, as would be expected for a half-metallic ferromagnet with four atoms in the primitive cell. Thus, unlike most of the other Co_2YZ Heusler compounds, Co_2CrIn cannot be a half-metallic ferromagnet. Finally, it should be noted that it was not possible up to now to stabilize other Co_2CrZ compounds in a pure $L2_1$ structure.

2.4.2 Tuning the Fermi Energy in the Middle of the Gap: From Co_2FeSi to $Co_2Mn_{1-x}Fe_xSi$ and $Co_2FeAl_{1-x}Si_x$

Due to insuperable problems such as disorder and the low magnetic moment of compounds containing Cr (and Al), we moved on to investigate new materials that clearly exhibit both the ordered $L2_1$ structure and a high Curie temperature. By inspecting the magnetic data of the known Heusler compounds in more detail, a very interesting aspect is found [33, 34]. A linear dependence is apparently obtained for Co_2-based Heusler compounds when the magnetic moments for the known, 3d metal-based Heusler compounds are plotted against their Curie temperatures (T_C) (see Fig. 2.3). According to this plot, T_C is highest for those half-metallic compounds that exhibit a large magnetic moment. By extrapolating from the linear dependence shown in Fig. 2.3, T_C is estimated to be above 1,000 K for compounds with 6 μ_B.

From the chemical point of view, it is clear that the exchange of Al by Si should lead to stronger covalent bonding. Indeed, Co_2FeAl does not exhibit a clean $L2_1$ structure but usually has a very high degree of $B2$-like and also $A2$-like disorder. Therefore, Co_2FeSi was revisited and its properties were analyzed in more detail. Indeed, it was found that Co_2FeSi exhibits the correct Heusler $L2_1$-type structure that is necessary for the occurrence of half-metallicity [34]. Using a Rietveld refinement, the lattice constant was determined by XRD to be 5.64 Å with an R_{Bragg} value < 5.5. A disorder between Co and Fe atoms (DO_3-type disorder) could be excluded from the XRD Rietveld refinement as well as from the EXAFS and neutron scattering data. During further structural and magnetic investigations, Mößbauer spectroscopy, EXAFS measurements, and both low and high temperature magnetometry were performed and all data analysis verified the high degree of order in Co_2FeSi, even on a short range scale, and excluded $A2$—or a $B2$-type disorder.

Low temperature magnetometry was performed to verify the estimated saturation moment. The measured magnetic moment in saturation was 5.97 μ_B at 5 K. An extrapolation to 6 μ_B per unit cell at 0 K perfectly fits the moment estimated from the Slater–Pauling rule. The experimental magnetic moment is supported by

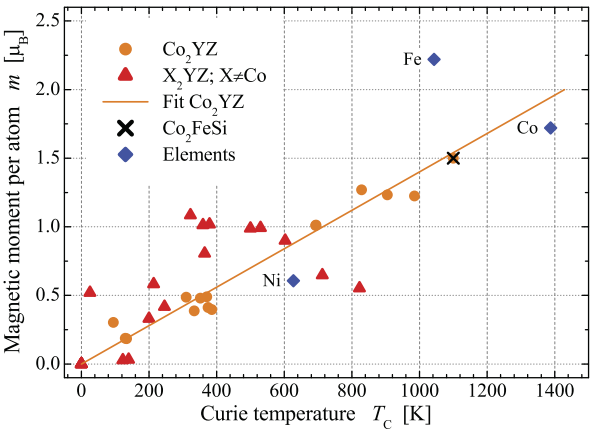

Fig. 2.3 Plot of the magnetic moment per atom of iron, nickel, cobalt, and selected Heusler compounds, as a function of the Curie temperatures. The *orange line* is a linear fit to the data for the Co_2YZ compounds

band structure calculations that indicate an HMF character with a magnetic moment of 6 μ_B. The high temperature magnetization of Co_2FeSi was measured using a vibrating sample magnetometer equipped with a high temperature stage. The ferromagnetic Curie temperature is found to be $T_C \approx 1100$ K. This value very well fits the linear behavior of T_C as a function of the magnetic moment for Co_2-based Heusler compounds (see Fig. 2.3). T_C is well below the melting point, which is determined using differential scanning calorimetry to be $T_m = 1{,}520$ K. In summary, the analysis shows that $L2_1$-ordered Co_2FeSi is a half-metallic ferromagnet that exhibits the highest values of Curie temperature and magnetic moment that have been reported for Heusler compounds.

On the other hand, next to Co_2FeSi, the Heusler alloy Co_2MnSi has attracted particular interest because it is predicted to have a large minority spin band gap of 0.4 eV and, at 985 K, has one of the highest Curie temperature, among the known Heusler compounds [35, 36]. Structural and magnetic properties of Co_2MnSi have been reported for films and single crystals [37–42]. In accordance with theoretical predictions, bulk Co_2MnSi has been stabilized in the $L2_1$ structure with a magnetization of 5 μ_B per formula unit. From tunneling magneto resistance (TMR) data with one electrode consisting of a Co_2MnSi film Schmalhorst et al. [43, 44] inferred a spin polarization of 61 % at the barrier interface. Although the desired spin polarization of 100 % was not reached, the experimental value of the spin polarization is larger than the maximum 55 % effective spin polarization of a variety of $3d$-transition metal alloys in combination with Al_2O_3 barriers [45]. However, the spin polarization of photoelectrons emerging from single crystalline Co_2MnSi films grown on GaAs by pulsed laser deposition indicate a quite low spin polarization at the Fermi level of only 12 % at the free surface [42]. Wang et al. [41, 42] assumed that partial chemical disorder was responsible for this discrepancy with the theoretical predictions.

Investigations [25, 30, 33, 46] of the electronic structure of Heusler compounds indicate that on-site correlation plays an important role in these compounds and

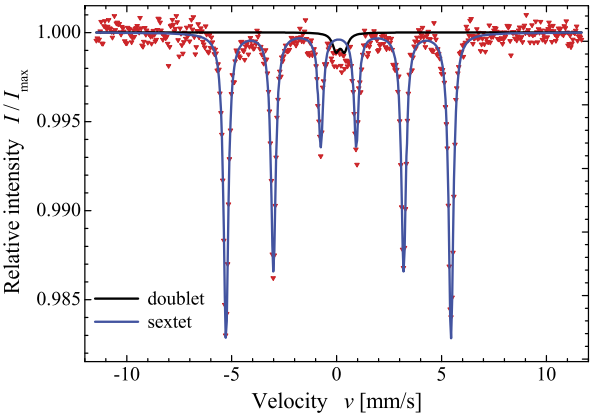

Fig. 2.4 ^{57}Fe Mößbauer spectrum of $Co_2Mn_{0.5}Fe_{0.5}Si$. The spectrum was taken at 290 K and excited by a ^{57}Co(Rh) source. *Solid lines* are results of a fit to determine the sextet and doublet contributions and to evaluate the hyperfine field

may serve to destroy the half-metallic properties of Co_2MnSi. In addition, if on-site correlation is considered in electronic structure calculations Co_2FeSi becomes a half-metallic ferromagnet with a magnetic moment of 6 μ_B.

A possible explanation is the position of the Fermi energy with respect to the minority band gap. A position close to the minority band edges (top of the minority valence band or bottom of the minority conduction band) might easily destroy the gap already at low temperatures without affecting the magnetic moment. One result from the electronic structure calculations on Co_2FeSi and Co_2MnSi is the indication of a shift of the Fermi energy from the top of the minority valence band (Y = Mn) to the bottom of the minority conduction band (Y = Fe) [47]. These particular positions of the minority gap with respect to the Fermi energy make both systems rather unstable with respect to their electronic and magnetic properties. Any small change in physically relevant quantities (e.g., lattice parameters) may easily serve to destroy the half-metallic character by shifting the Fermi energy outside of the minority gap. Therefore, the substitutional series of the quaternary Heusler compound $Co_2Mn_{1-x}Fe_xSi$ was synthesized and investigated both experimentally and theoretically. All samples of the substitutional series exhibit an $L2_1$ order that is independent of the Fe concentration x. The observed structural order-disorder phase transition from $L2_1 \leftrightarrow B2$ is nearly independent of x and occurs at about 1030 K. Mößbauer measurements show only a negligible paramagnetic contribution confirming the high degree of order over the whole substitutional series (see Fig. 2.4).

In agreement with the expectation from the Slater–Pauling curve, the magnetic moment increases linearly with x from 5 μ_B to 6 μ_B. True bulk sensitive, high energy photo emission bearded out the inclusion of electron–electron correlation in the calculation of the electronic structure and gave an indirect advise on the gap in the minority states. Both valence band spectra and hyperfine fields indicate an increase of the effective Coulomb exchange parameters with increasing Fe concentration. The calculated band structures suggest that the most stable compound in a half-metallic state will occur at an intermediate Fe concentration. From both the experimental and computational results it is concluded that a compound with an in-

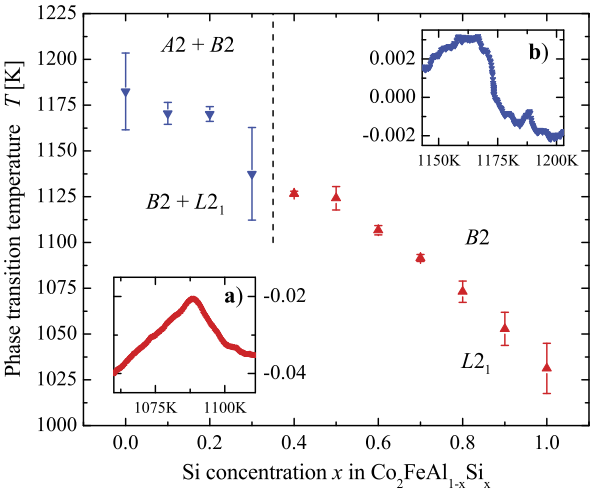

Fig. 2.5 Phase transitions in $Co_2FeAl_{1-x}Si_x$. Shown is the composition dependence of the phase transition temperature. The length of the vertical bars corresponds to the experimental hysteresis (see text). The insets (**a**) and (**b**) display typical DSC curves in high ($x = 0.7$) and low ($x = 0.1$) Si content compounds, respectively

termediate Fe concentration of about 50 % should be most stable and best suited for spintronics applications.

The end members of this series, Co_2FeSi and Co_2MnSi, have been used for fabrication of magnetic tunnel junctions [48–50]. The tunnel magnetoresistance ratios of 159 % in the Mn compound at low temperature and 41 % in the Fe compound at room temperature suggest that still an improvement with respect to the temperature stability of the TMR is necessary.

In $Co_2Mn_{1-x}Fe_xSi$ the transition metal carrying the localized moment is exchanged. This might lead to unexpected effects on the magnetic properties if the samples are not completely homogeneous. The situation is different in the isoelectronic series $Co_2FeAl_{1-x}Si_x$ where the main group element is substituted. Tezuka et al. [51, 52] reported about TMR junctions build from $Co_2FeAl_{0.5}Si_{0.5}$. The junctions exhibited TMR ratios of 76 % at 300 K and 106 % at 5 K for the $B2$ structure while the junctions with $L2_1$ structure showed 51 % and 78 % at 300 K and 5 K, respectively. The TMR ratio is 175 % at 300 K for optimized junctions with $L2_1$ structure [52] and thus larger than the ones found for pure Co_2FeAl or Co_2FeSi electrodes.

Recent ab-initio calculations [53] indicated that the compound with 50 % of the Al substituted by Si will lead to a situation where ε_F is located close to the middle of the minority gap and thus should lead to an improved temperature stability of the spin polarization, in particular if quasi particle excitations are appearing close to the band edges. The following study is devoted to the bulk properties of $Co_2FeAl_{1-x}Si_x$ in order to find the most stable compound of the series with respect to the structural and magnetic properties and thus the most promising candidate for thin film devices using them in GMR and TMR applications.

Differential scanning calorimetry (DSC) was used to find the high temperature phase transitions in the substitutional series. Figure 2.5 displays the dependence of the order-disorder transition temperature as a function of the Si concentration x. The

insets display the change of the DSC signal as a function of the temperature using nominal heating rates of 15 K min^{-1}. Depending on the temperature rates and the actual amount of material, a shift of the maxima is observed between heating and cooling curves (see also [47]) that is mainly due to an intrinsic hysteresis effect of the method. The length of the vertical bars in Fig. 2.5 corresponds to the range of that hysteresis. The signal at the phase transition is rather high for $x > 0.4$ (Fig. 2.5(a)), that is, for compounds exhibiting clearly the $L2_1$ structure. In that case the signal can be clearly attributed to an $L2_1 \leftrightarrow B2$ order-disorder phase transition as also observed in other quaternary Heusler compounds [47, 54]. For $x < 0.4$ the signal is much weaker.

Here, XRD indicates mainly a $B2$ structure with a very low portion of $L2_1$ and in some cases a high portion of an $A2$ structure. Therefore, the signal at low x may be attributed either to an $L2_1 \leftrightarrow B2$ or to a $B2 \leftrightarrow A2$ phase transition. Overall, Fig. 2.5 demonstrates that the structural transition temperature of the $L2_1$ to the $B2$ phase $T_t^{B2 \leftrightarrow L2_1}$ decreases almost linearly with increasing Si content at least for $x > 0.4$. The results from both, XRD and DSC, demonstrate the better structural stability of the compounds with high Si content. This is expected from the stronger hybridization between Co and Si in these compounds [53]. An important detail is that for $x > 0.5$ the as-cast samples exhibit the $L2_1$ structure which make the production of thin films much easier because it may avoid extensive heat treatment to reach the correct structure of the samples.

In summary, the series $Co_2FeAl_{1-x}Si_x$ crystallizes for $x \geq 0.4$ in the $L2_1$ structure. This structure is essentially required for a high spin polarization resulting in high magnetoresistive effects. Both, structural and magnetic investigations suggest that the Si rich systems $x > 0.5$ are more stable with respect to the $L2_1$ structure, due to the stronger hybridization between Co and Si compared to Al. For $x \approx 0.5$, calculations predict that the Fermi energy is located in the middle of the gap of the minority states [53] while in Co_2FeSi ε_F is located at the bottom of the conduction band which can easily destroy the half-metallicity. This behavior will make $Co_2FeAl_{0.5}Si_{0.5}$ stable against temperature variations. From the combination of experimental (better order for high Si content) and theoretical findings (robust gap at $x \approx 0.5 \pm 0.25$) it is concluded that a compound with an intermediate Si concentration close to $x = 0.5 \ldots 0.7$ would be best suited for spintronics applications, especially for GMR and TMR applications.

Very recently, the half-metallicity of $Co_2FeAl_{0.5}Si_{0.5}$ at room temperature was demonstrated experimentally by Shan et al. [55]. Furubayashi et al. [56] reported on the structure and transport properties of current-perpendicular-to-plane spin valves (CPP-SV) with $Co_2FeAl_{0.5}Si_{0.5}$ or Co_2MnSi Heusler alloy magnetic layers and an Ag spacer layer. The CPP GMR values of 12.4 % at RT and 31 % at 12 K were measured from an optimally annealed SV with $Co_2FeAl_{0.5}Si_{0.5}$/Ag/$Co_2FeAl_{0.5}Si_{0.5}$ trilayer. On the other hand, both the upper and lower Co_2MnSi layers were $L2_1$ ordered in the SVs using Co_2MnSi/Ag/Co_2MnSi. MR ratios of 11.9 % at RT and 20 % at 10 K were obtained. This two results emphasize the high suitability of well designed Co_2-based Heusler compounds for spintronics applications.

2.4.3 Solving the Problem of Structure Determination in 3*d* Transition Metal-Based Heusler Compounds by Means of Anomalous X-Ray Diffraction

This section reports on the investigation of the structural properties of the 3*d* transition metal-based Heusler compounds Co_2FeZ with Z = Ga, Ge, and $Ga_{0.5}Ge_{0.5}$. The high Curie temperatures and magnetic moments make them suitable candidates for spintronics applications [57, 58]. For the predicted high spin polarization and half-metallic character of those compounds it is necessary that the samples crystallize in the $L2_1$ structure. Due to the very similar scattering factors of the constituents it is not possible to distinguish the correct structure with commonly used X-ray sources, even if the compounds crystallize in the correct $L2_1$ structure.

Most of the X_2YZ Heusler compounds used in the production of TMR devices are based on 3*d* transition metals like Co for the X element and Cr, Mn, Fe, or mixtures of those for the Y element. The main group element (Z) is usually taken from the third (Al, Si) or from the fourth row (Ga, Ge) of the periodic table. The detection of the correct structure, as a necessary prerequisite for a half-metallic character, by regular X-ray diffraction (XRD) is difficult especially if all three elements in the compound are from the fourth row. In that case, the scattering factors of all three elements are very similar for excitation by standard laboratory sources (for example: Cu K_α or Mo K_α).

Various Heusler compounds appear not only in an ordered structure but also exhibit pronounced alloying. Besides the $L2_1$ structure of ordered X_2YZ compounds, the most commonly occurring types of disordered alloy have the $B2$ (CsCl-type with complete mixing of Y and Z atoms resulting in $X(Y_{0.5}Z_{0.5})$ or the $A2$ (W-type with complete mixing of all types of atom resulting in $(X_{0.5}Y_{0.25}Z_{0.25})$) structure. In particular, when all elements are taken from the fourth row of the periodic table one needs a unambiguous method to prove the $L2_1$ structure.

Ravel et al. [59] used the method of anomalous XRD to determine antisite disorder with a high precision, in particular for thin films of the Heusler compound Co_2MnGe. This technique has also been successfully used to determine the crystallographic polarity of ZnO epilayers [60], to observe an increase of the structural order parameter in Fe–Co–V soft magnetic alloy after thermal ageing [61], and to distinguish between alloying and segregation in CoCrPt films [62]. In the present work, the method of anomalous XRD is used to determine the structure in 3*d* transition metal-based Heusler compounds where the constituents have almost the same scattering factors and therefore the structure determination with commonly used X-ray sources in the laboratory failed.

The structure factors for an ordered $L2_1$ compound and disordered $B2$ and $A2$ alloys and the results for the (111) and (200) reflections are summarized in Table 2.1. (Note that the indexing of the fcc lattice was used here for all three cases, independent of the present symmetry that is for $A2$ and $B2$ different from $L2_1$.) The (111) reflex appears here only in the $L2_1$ but not in the disordered $A2$ or $B2$ structures. Therefore, the present work is concentrated on the (111) reflection. The factor for

Table 2.1 Structure factors for the ordered $L2_1$ compound and the disordered $B2$ and $A2$ alloys. Note that one has in Heusler alloys $A = X_{1/2}Y_{1/4}Z_{1/4}$ for the $A2$, or $B = Y_{1/2}Z_{1/2}$ for the $B2$ structure. The positions a, b, c, and d correspond to $(0, 0, 0)$, $(\frac{1}{2}, \frac{1}{2}, \frac{1}{2})$, $(\frac{1}{4}, \frac{1}{4}, \frac{1}{4})$, and $(\frac{3}{4}, \frac{3}{4}, \frac{3}{4})$, respectively

	a	b	c	d	f_{111}	f_{200}
$L2_1$	Z	Y	X	X	$f_Y - f_Z$	$f_Y + f_Z - 2f_X$
$B2$	B	B	X	X	0	$2(f_B - f_X)$
$A2$	A	A	A	A	0	0

the (220) reflection is in all three cases $f_{220} = 2f_X + f_Y + f_Z$. It is seen that the factor f_{111} of the $L2_1$ structure becomes very small if the Y and Z atoms behave similarly, as is the case if both atoms are from the fourth row and have nearby N, like Fe and Ga. In that case the ordered structure is almost indistinguishable from the disordered ones.

The situation changes if one approaches the photon energy close to the absorption edges of the constituents, because then the anomalous scattering factors play an important role. The complete scattering factors of the atoms with ordinal number N are described by

$$f_N = f_0(N, \theta, E) + \big(f'(N, E) + if''(N, E)\big), \tag{2.1}$$

where $f'(N, E)$ and $f''(N, E)$ are the real and imaginary part of the anomalous scattering factor. These factors do not depend on the scattering geometry but only on the photon energy (E) and the material (N).

Figure 2.6(a) displays the calculated anomalous scattering factors of Co, Fe, and Ga. For better comparison, the real part of the anomalous scattering factor $f_1 = N + f'$ is shown in the Hanke-form with the limiting value of the regular scattering factor ($\lim f_0(N, \theta, E) = N$) added.

Figure 2.6(b) displays the calculated anomalous scattering intensities for Co_2FeGa using f_1 and f_2 from Fig. 2.6(a), that is, the dependence on the scattering angle is not respected. The enhancement of the (111) reflection (Fig. 2.6(c)) indicating the $L2_1$ structure is clearly visible at energies close to the Fe K-edge.

Figures 2.6(d), (e), and (f) show the XRD data (for better comparison here only the (111) reflexes) taken at $h\nu = 7050$ eV and at the Fe K-edge ($h\nu = 7111.96$ eV) for $Co_2FeGa_{0.5}Ge_{0.5}$, Co_2FeGe, and Co_2FeGa, respectively. The enhancement of the (111) reflections when using excitation energies close to the Fe K-edge is clearly visible and fits the theory. This is clear proof of the ordered $L2_1$ for these compounds which was not possible with a standard XRD lab sources.

Before measuring the anomalous XRD data, EXAFS measurements of the samples were performed. From this experimental data the anomalous scattering factors f' were directly derived using the DIFFKK program developed by Cross et al. [63] and the excitation energies used then for the anomalous XRD were taken. Figures 2.7(a), (b), and (c) show the EXAFS data at the Fe, Co, and Ga K-edges, respectively, from Co_2FeGa and Figs. 2.7(c), (d), and (e) show the derived f's, respectively.

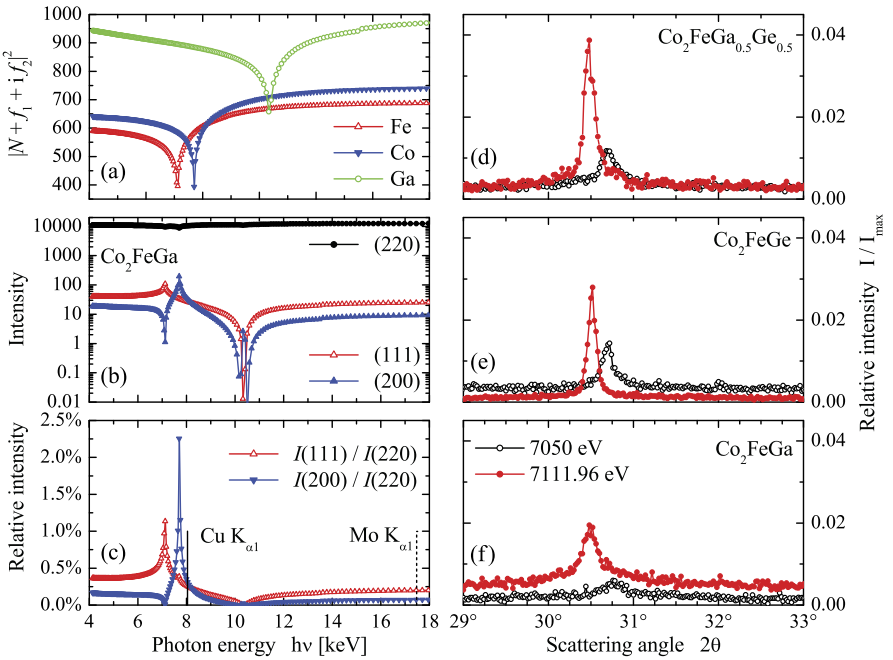

Fig. 2.6 Comparison between theory and the experiment. (**a**) shows the anomalous scattering factors of Co, Fe, and Ga. (**b**) and (**c**) show the calculated anomalous XRD intensities for Co_2FeGa. The energies for excitation by typical laboratory sources are assigned by *vertical lines* in (**c**). (**d**), (**e**), and (**f**) show the XRD data taken at $h\nu = 7050$ eV (*open circles*) and at the Fe K-edge (*closed circles*) for $Co_2FeGa_{0.5}Ge_{0.5}$, Co_2FeGe, and Co_2FeGa, respectively

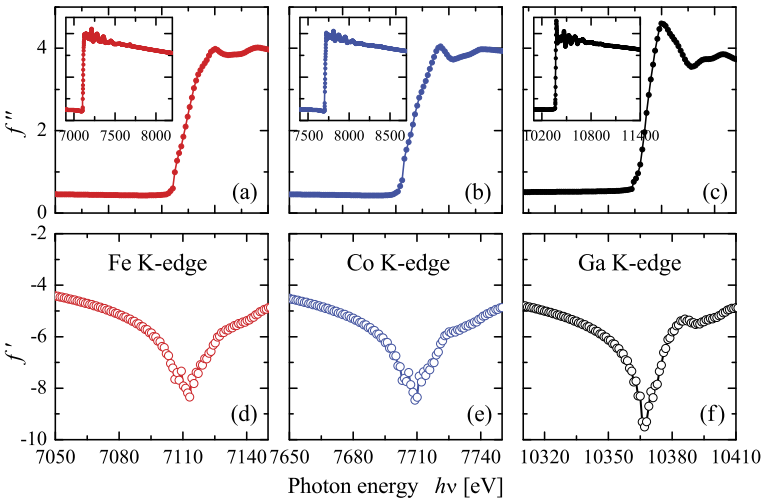

Fig. 2.7 EXAFS data from Co_2FeGa. (**a**), (**b**), and (**c**) show the EXAFS data around the Fe, Co, and Ga K-edges, respectively. The *insets* show the complete measurement. (**c**), (**d**), and (**e**) show the derived f's, respectively

In summary, it has been shown that synchrotron radiation techniques can solve the problem of crystallographic structure determination, even in the case where the scattering factors of elements in a compound are very similar in response to excitation by traditional lab sources. Knowing the anomalous scattering factors for the compounds, one can use anomalous XRD to determine the correct crystallographic structure of the sample. It was shown by other groups that this technique works quite well as well for thin film samples [59–62] so it is expected that the combination of EXAFS and anomalous XRD may also lead to a better understanding of the structure of multilayer thin films in order to improve the quality of TMR-junctions.

A large amount of other new Heusler compounds were synthesized and investigated using various different techniques to analyze their suitability as new materials for spintronics applications [64]. The prepared compounds contain ternary Cr-, Rh-, Ru-, Ni-, Pd-, and Pt-based Heusler systems as well as quaternary Co_2-based compounds and compounds of the general formula $XX'YZ$.

2.5 Highly Ordered, Half-Metallic Co_2FeSi Single Crystals

As already mentioned above, several MTJs of Co_2FeSi have successfully been fabricated, yielding a large TMR. However, in many cases the TMR is strongly temperature dependent, e.g. in Co_2FeSi and Co_2MnSi based MTJs [65–68]. According to Chioncel et al., the strong temperature dependence arises from nonquasiparticle states and their crucial contribution to the finite-temperature spin polarization [69]. In order to separate such extrinsic effects from possible intrinsic contributions to the temperature dependence of the TMR, the investigation of high quality single crystals is indispensable. Therefore, the next section reports about highly ordered, half-metallic Co_2FeSi single crystals.

Two different single crystals were prepared. One was grown by the Czochralski method using a Centor Vacuum Industries Series Crystal Puller. Metallographic investigations of polished pieces of the Czochralski grown single crystal revealed single crystalline areas of 2–3 mm width and 5–7 mm length.

The other single crystal was grown by the optical floating zone technique. Zone melting was carried out in a GERO SPO optical floating zone furnace with two 1000 W halogen lamps with the radiation focused by ellipsoidal, gold coated mirrors. To avoid oxidation the furnace was flushed with 5.0 purity argon for several hours, and during growth a gas flow rate of 300 ml/min of argon with 2 % hydrogen was maintained. The seed and feed rods were counter rotated at 45 and 15 rpm, respectively, the growth speed was set at 20 mm/h. Metallographic investigations revealed the single crystal to be about 1–3 cm long and to have nearly the width of the whole rod, except a thin layer at the surface of the freshly grown crystal, which contains some small additional grains.

Laue diffraction with a spot size of 2 mm $\times$ 2 mm was performed on the floating zone crystal with 25 kV incident copper radiation at 20 mA in reflection geometry. The resulting diffraction patterns (see Fig. 2.8) were compared with simulations

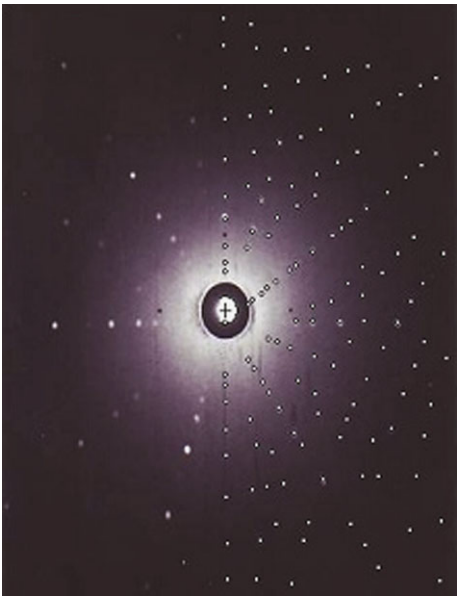

Fig. 2.8 Laue diffraction pattern of the zone molten single crystal. In addition, the simulated diffraction pattern assuming $Fm\bar{3}m$ symmetry and a lattice constant of 5.66 Å is represented by *bright dots* on the *right side* of Fig. 2.8. The perfect matching between the measured diffraction pattern and the simulation demonstrates single crystalline nature and a high degree of order of the zone melted single crystal

(bright dots on right side of Fig. 2.8). The good match verifies the single crystalline nature of the sample. High quality $L2_1$ ordering in space group $Fm\bar{3}m$ with a fitted unit cell parameter of 5.66 Å is confirmed, which is in good agreement with previous results [30]. The simulation also confirms the crystal growth along the (110) axis without twinning.

All crystals show metallic behavior in the resistivity measurements, see Fig. 2.9(a). As expected, the resistivity decreases with decreasing temperature in the temperature range between 300–50 K. Remarkably, the resistivity below 50 K is temperature independent, in agreement with the results of Ambrose et al. [70]. The residual resistivity at 2 K is 0.0155 μΩ m for the floating zone single crystal, 0.0344 μΩ m for the polycrystal and 0.134 μΩ m for the Czochralski grown single crystal, respectively. Note that all measurements of the electrical resistivity shown here are well below the Curie-temperature reported to be 1100 K for Co_2FeSi [30].

The residual resistivity ratio (RRR, here $\rho_{300\,\mathrm{K}}/\rho_{2\,\mathrm{K}}$) is a measure of the quality of a crystal [37]. Good ordering is inferred in both the zone melted and the polycrystal by the RRR of 5.2 and 5.9, respectively. The RRR values reported here are on the same order of magnitude as found in a Co_2MnSi single crystal (6.5), which the highest RRR reported for a Heusler compound [37, 71]. The RRR of the Czochralski grown crystal is lower by a factor of 2 and relatively poor performance compared to the zone melted and polycrystal, indicating a lower degree of order, in line with our NMR results. However, all RRR presented here indicate excellent crystallinity and homogeneity compared to previously reported RRR for Heusler compounds or alloys in general (see e.g. [38, 70, 72, 73]). The observation of a higher resistivity in the polycrystal compared to the floating zone single crystal might arise from mi-

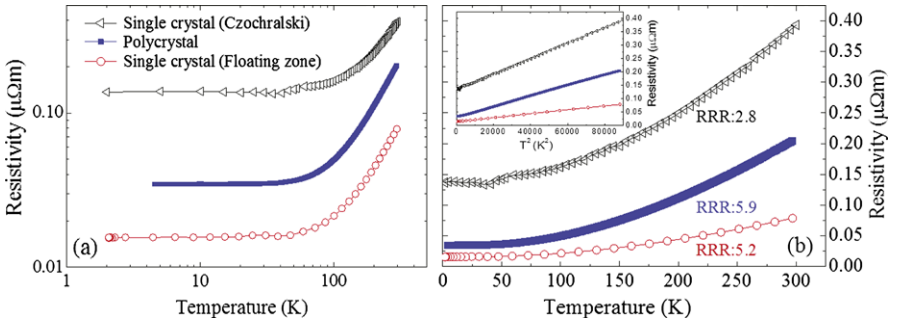

Fig. 2.9 (**a**) Resistivity as a function of temperature on a logarithmic scale to show the plateau at temperatures below 50 K. (**b**) Resistivity as a function of temperature for the Czochralski grown single crystal (*triangles*), the polycrystal (*squares*) and the zone melted single crystal. The *inset* shows the resistivity as a function of T^2 to demonstrate the linear dependence and, thus, the T^2 power law dependence of the resistivity as a function of temperature

croscopic cracks at the grain boundaries present in the polycrystal, leading to longer transport paths.

Figure 2.9(a) shows the resistivity as a function of temperature on a logarithmic scale to demonstrate the temperature independence of the resistivity below 50 K. Above 50 K, the resistivity curves of all crystals follow a T^N power law (fit not shown here), where $N = 1.9$ for the zone molten single crystal, $N = 2.1$ for the polycrystal and $N = 1.6$ for the Czochralski grown single crystal, respectively. The resistivity for all three crystals is reasonably well described by an appropriate T^2 behavior in the high temperature regime, a transition regime and the temperature independent regime below 50 K, while the range of the transition regime is slightly different for the different crystals. The resistivity curves of the zone molten single crystal and the polycrystal approximately scale with each other by a factor of 2.55. The validity of the T^2 behavior in the high temperature regime is further confirmed by a plot of the resistivity as a function of T^2, demonstrating a linear dependence (see inset of Fig. 2.9). A T^2 behavior is expected for a conventional ferromagnet due to coherent one-magnon scattering processes [74]. Assuming one-magnon scattering of conduction electrons, there must be the possibility for spinflips, and thus, both the spin-up and the spin-down electrons are present at the Fermi-level [74]. Consequently, one expects the absence of one-magnon scattering in half-metallic ferromagnets, where only one spin channel contributes to the electrical transport. The absence of any T^2 contributions at temperatures below 50 K might suggest the absence of a one-magnon channel and thus half-metallic ferromagnetism in Co_2FeSi at temperatures below 50 K. The cross-over to more conventional ferromagnetic transport behavior above 50 K indicates the onset of spin scattering which needs to be taken into account (besides interface and impurity scattering) for understanding the temperature dependence of the tunneling magnetoresistance in Co_2FeSi devices [48, 50, 65, 68, 75, 76].

In summary, excellent crystals of the $L2_1$ ordered half-metallic Heusler compound Co_2FeSi confirmed by Laue diffraction, NMR (not shown here, see [77] for

details) and the residual resistivity were obtained. The ratio between the residual resistivity at 300 K and 2 K is on the same order of magnitude as the best residual resistivity ratio previously reported for a Heusler compound. The resistivity as a function of temperature roughly follows a T^2 behavior in the high temperature regime, as expected for ferromagnets. Remarkably, the resistivity is temperature independent at low T, which might indicate half-metallic ferromagnetism of Co_2FeSi in the low temperature regime. The synthesis of such high quality Heusler single crystals opens a promising route to exploit the rich physical properties that are realized in various Heusler compounds.

2.6 Heusler Compounds with 4*d* Valence Electrons

Most of the work being reported above was concentrated on the Co_2-based Heusler compounds, whereas compounds based on 4*d* transition metals are rarely investigated. There are only a few results published on the two series $Ru_{2-x}Fe_xCrSi$ [78], and $Ru_{2-x}Fe_xCrGe$ [79]. These compounds exhibit the $L2_1$ structure but the reported saturation magnetization is lower than that predicted by theory. A reason for this could be that these compounds contain Cr, and the magnetic moment of Cr is reduced, as in the $Co_2Cr_{1-x}Fe_xAl$ series, because of complete, or at least partial, ferrimagnetic order (antiparallel orientation of the moments of different Cr atoms, or between X and Cr atoms). Therefore, several Heusler compounds based on 4*d* transition metals that contain other 3*d* transition metals instead of Cr on the Y position were synthesized.

2.6.1 Investigation of Rh_2MnGe

Two very well investigated Heusler alloys are Co_2MnZ (Z = Si and Ge) with a calculated band gap of 0.4 eV [35] to 0.8 eV [80] and a high Curie temperature above 900 K [36]. A strong hybridization of the Mn and Co 3*d* states in this system causes the Mn 3*d* states being itinerant to a certain degree [81]. In this section we report about investigation on the isoelectronic alloy Rh_2MnGe with 29 valence electrons per formula unit as in the case of Co_2MnGe. The main difference between Rh_2MnGe and Co_2MnGe is given by the smaller width of the Rh 4*d* states relative to the Co 3*d* states and the larger lattice constant of the Rh-based system. The Mn atom is effectively oversized because of the strongly widened lattice due to the large Rh atoms. The hybridization between the Rh and Mn atoms is smaller than between the Co and Mn atoms and the majority/minority spin splitting for Mn is strongly favored. Therefore, Rh_2MnZ compounds are discussed as systems with fully localized magnetic moments, in contrast to the Co_2MnZ-type compounds where the Co magnetic moment can obviously not be neglected. The gap in the minority-spin states of Co_2MnZ is also predicted for Rh_2MnZ but this gap apparently becomes broader and the Fermi level is no longer found in the gap [82] and the total magnetic moment is not expected to be an integer number.

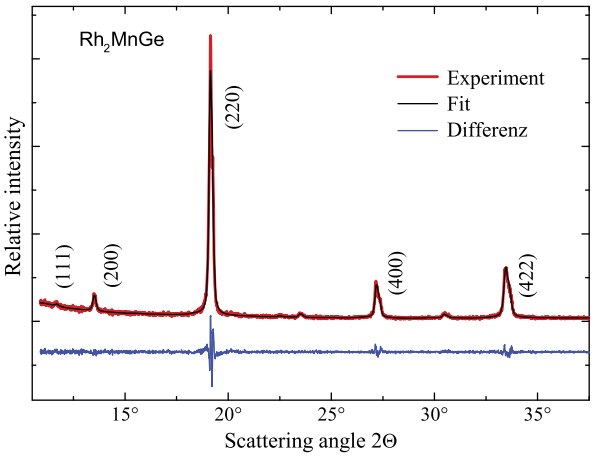

Fig. 2.10 X-ray powder diffraction pattern in Bragg–Brentano geometry for Rh_2MnGe, indicating an $L2_1$ structure. The simulated pattern and the difference between measured and simulated pattern are given for comparison

Structural characterization has been performed with XRD of powders. Due to the larger differences of the scattering factors between Rh, Mn and Ge, XRD provides a slightly better structural information compared to e.g. Co_2MnGe. The strong sharp (220)-peak confirms the presence of a single cubic phase. The comparatively small (10 % of the (220)-peak) (111) and (200) superstructure peaks (see Fig. 2.10) are decisive for the $L2_1$ Heusler structure. The simulated powder diffraction pattern of Rh_2MnGe shows the expected peaks for the defect-free structure. These superlattice peaks both vanish for the case of randomly occupied lattice sites ($A2$ structure). In the case of randomly occupied Mn sites with Mn and Ge ($B2$) only the (200) superlattice peak would be seen, while the (111) peak vanishes. A quantitative evaluation of the spectra limits the disorder to less than 10 % contribution of the $B2$ structure with a lattice parameter of 6.04 Å.

Additionally, XAS and XMCD spectra at the Rh $M_{3,2}$ edges and at the Mn $L_{3,2}$ edges have been measured of the ferromagnetic Heusler alloy Rh_2MnGe. The Rh spectrum shows no multiplet features and can be reproduced by LDA calculations. From this observation we conclude that the Mn moment is strongly localized. The Rh moment is an order of magnitude smaller than the Mn moment. The temperature dependence of the Mn and Rh moments is almost equal to each other. The contribution of the orbital magnetic moment is very small for both elements with orbital to spin moment ratios of 0.01 ± 0.02 for Mn and 0.20 ± 0.15 for Rh. For more details about the XAS and XMCD investigation of Rh_2MnGe see the chapter about XMCD and [83].

2.6.2 *Investigation of Ru_2YZ*

Half-metallic system with 24 valence electrons are of great interest because of their predicted semiconducting nature. In a similar vein, two new half-metallic Heusler

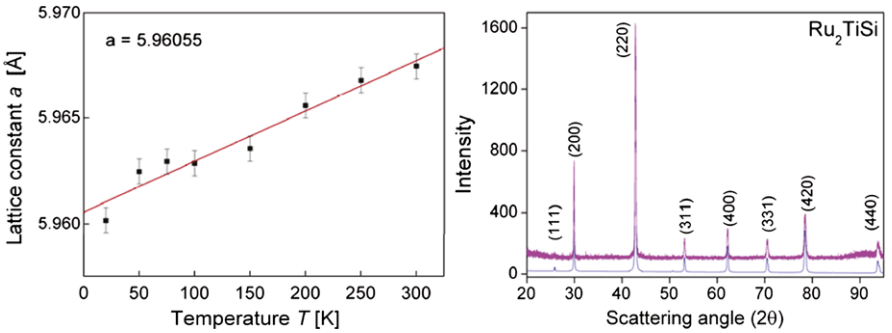

Fig. 2.11 XRD spectrum for Ru_2TiSi. The spectrum was excited by Cu-K_α radiation (*right*). Temperature dependency of the cubic cell volume V for Ru_2TiSi (*left*). The fit of the data to $a(T^3)$ dependence is shown as a *full line*

compounds namely Ru_2TiSi and Ru_2VAl with 24 valence electrons were synthesized.

The crystalline structure was determined by XRD using Cu-K_α radiation. Ru_2TiSi exhibits the $L2_1$ structure. The (111) superstructure reflection is not very strong and is very hard to see. Typical powder diffraction patterns are shown in Fig. 2.11(right). The lattice parameter found from the Rietveld-refinement is $a = 5.96$ Å.

Additionally, the structural parameter of Ru_2TiSi has been investigated in dependence of the temperature between 20 K and 300 K. Figure 2.11(left) shows the temperature dependency of the cell volume $V = a^3$ of the cubic cell. The volume decreases by about 0.5 % if the temperature is lowered from room temperature to 20 K. The change of the cell volume with temperature is clearly non-linear and evidence is given that the volume increases with an approximate T^3 law.

The Ru_2VAl compound exhibits a $B2$ structure, only the (200) superlattice peak of the $B2$ structure type was observed, while the (111) peak was vanished. This type of disorder shows up as a (200) superlattice peak with higher intensity than the (111) peak. The lattice parameter found from the Rietveld-refinement is $a = 5.99$ Å.

Both compounds are—as expected from the Slater–Pauling rule—diamagnetic, which was confirmed by various SQUID measurements.

2.7 Quaternary Heusler Compounds

In the following section, the properties of the $CoFe_{1+x}Ti_{1-x}Al$ and $CoMn_{1+x}V_{1-x}Al$ solid solutions are investigated. It is expected that the partial replacement of Ti by additional Fe or V by additional Mn will keep the $F\bar{4}3m$ and one has a transition from the Y to the X structure rather than to the $L2_1$ structure. The pure compounds $x = 0$ carry 24 valence electrons in the primitive cell and are expected to exhibit no net magnetic moment. Therefore, the onset of the magnetic phenomena with increasing valence electron concentration can be studied by the degree of substitution.

An advantage is that the particular way of quaternary substitution as used here does not change the crystal symmetry either global or local.

2.7.1 Structural Properties of $CoMn_{1+x}V_{1-x}Al$ and $CoFe_{1+x}Ti_{1-x}Si$

For the pure compounds CoFeTiAl and CoMnVAl (XRD not shown here) the *fcc* typical (111) and (200) reflections appear in the XRD pattern of both compounds. No impurities are detected by XRD. A refinement of the data reveals the lattice parameter $a_{\mathrm{FeTi}} = 5.8509$ Å for CoFeTiAl and $a_{\mathrm{MnV}} = 5.8045$ Å for CoMnVAl, both at 300 K. The best R-values were obtained for the Y structure (CoFeTiAl: $R_p = 6.6$; $R_{wp} = 8.7$ and CoMnVAl: $R_p = 7.2$; $R_{wp} = 9.9$). The difference between measured and refined data shows some deviation at the (200) reflection that might be caused by a small amount of disorder. However, a fit for the X structure with intermixing of Fe and Ti or Mn and V has worth results with R_p (R_{wp}) being larger by 0.3 (1.0) for both compounds. Other types of disorder—that are swapping of Co–Ti, Co–V, or any intermixing of Al with one of the transition metals—were leading to much higher R values and can be excluded as possible types of disorder. Only Co–Fe or Co–Mn interchange or a slight deficiency of Al results in R-values similar or slightly lower compared to the pure Y structure. However, it is not possible to distinguish either these two types of disorder or the correct amount of disorder from measurements at one single photon energy. The reason is that the number of parameters for the fit becomes larger than the number of distinguishable reflections.

Figure 2.12 compares the XRD data of the two series $CoFe_{1+x}Ti_{1-x}Al$ and $CoMn_{1+x}V_{1-x}Al$. The *fcc* typical (111) and (200) reflections are small as already observed for the pure compounds. However, they are clearly resolved in most of the samples. The (111) reflection is absent in $CoFe_{1.5}Ti_{0.5}Al$ what is explained by antisite disorder. As for the pure compounds, the particular type of disorder cannot be determined from measurements at one single photon energy. The lattice parameter stay unchanged within the error of the measurement. This points out that the lattice parameter is dominated by the Co–Fe and Co–Mn sub-lattice interaction rather than by the interaction between transition metal and main group element.

2.7.2 Magnetic Properties of $CoMn_{1+x}V_{1-x}Al$ and $CoFe_{1+x}Ti_{1-x}Si$

The magnetic moment m of Heusler compounds, especially Co_2-based half-metallic ferromagnets, follows the Slater–Pauling rule where one has for localized moment systems an average magnetic moment (in multiples of the Bohr magneton μ_B) per atom of:

$$m_{av} = n_{av} - 6 - 2n_{sp}. \tag{2.2}$$

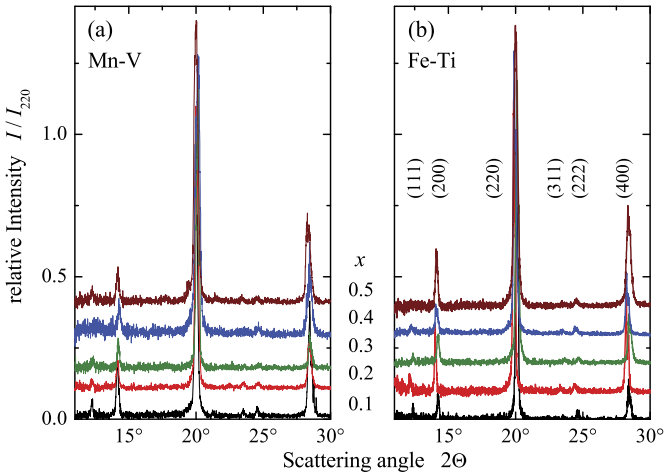

Fig. 2.12 XRD data of $CoMn_{1+x}V_{1-x}Al$ (**a**) and $CoFe_{1+x}Ti_{1-x}Al$ (**b**). The data are taken with Mo K_α radiation and normalized to the intensity of the (220) reflection. Data for $x > 0.1$ are plotted with an offset for better comparison

n_{av} is the mean number of valence electrons per atom in an alloy or compound and n_{sp} arises from the average number of unbalanced minority sp electrons. The number six arises from the fact that the d electrons are constrained such that the Fermi energy falls into a minimum (or gap) between occupied and unoccupied d states and therefore minimizes the total energy. In half-metallic ferromagnets with a gap in one of the spin densities or in quasi closed shell compounds all sp electrons are occupied and the n_{sp} term vanishes. In 2:1:1 or 1:1:1:1 Heusler compounds one has four atoms in the primitive cell and thus an overall magnetic moment of

$$m = (N_v - 24)\mu_B. \tag{2.3}$$

N_v is the accumulated number of valence electrons in the primitive cell (for details see [57, 81, 84, 85]). Here one has $2 + n(d)$ for each transition metal and $2 + n(p)$ for the main group element, where two arises in both cases from the s electrons and $n(d)$ and $n(p)$ are the numbers of available d and p valence electrons, respectively. At $N_v = 24$ the materials are not ferromagnetic according to the Slater–Pauling rule. The reason is that a quasiclosed shell character is reached at $N_v = 24$. It is caused by successive filling of the $a1, t1$, (two s, six p electrons) $e, t2$ (ten d electrons) bands, followed by subsequent complete filling of an additional $t2$ band (six d electrons). Deviations from (2.3) will appear when the compound is not in a half-metallic state and unbalanced sp or d electrons are present. For some of the $L2_1$ ordered compounds, 24 valence electrons lead to the phenomenon of half-metallic completely compensated ferrimagnetism [86], where the moments are ordered in a way that the total magnetic moment vanishes even though individual magnetic moments have-contrary to antiferromagnets—different magnitudes [87].

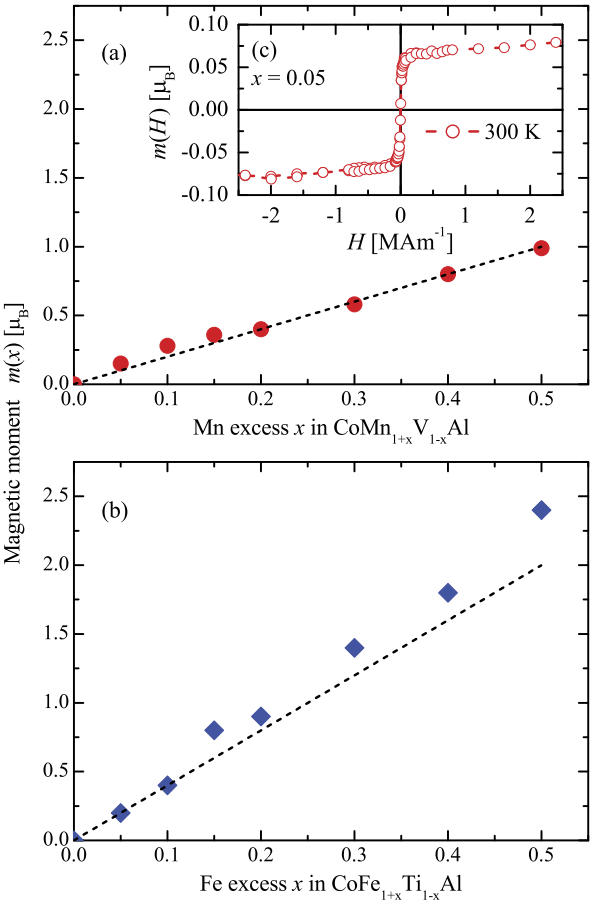

Fig. 2.13 Magnetization data of CoT'$_{1+x}$T"$_{1-x}$Al. Shown is the concentration dependence of the saturation magnetic moments of $CoMn_{1+x}V_{1-x}Al$ in (**a**) and of $CoFe_{1+x}Ti_{1-x}Al$ in (**b**). The measurements were performed at 5 K. The *lines* correspond to the expected values from the Slater–Pauling rule. The *inset* (**c**) shows the hysteresis of $CoMn_{1.05}V_{0.95}Al$ measured at 300 K

The magnetic data of the two series $CoFe_{1+x}Ti_{1-x}Al$ and $CoMn_{1+x}V_{1-x}Al$ are compared in Fig. 2.13.

The inset (c) in Fig. 2.13(a) shows the hysteresis of $CoMn_{1.05}V_{0.95}Al$ measured at 300 K. This demonstrates that the Curie temperature is above room temperature already at the lowest Mn substitution of 5 %. Similar to this composition, all samples of both series exhibited for $x > 0.05$ a ferromagnetic type hysteresis at 300 K. The shape of the hysteresis was in all cases soft-magnetic as for the shown sample. From the Slater–Pauling rule one expects that the saturation magnetization m increases with the concentration x and the given difference in the number of valence electrons by

$$m(x) = (\Delta N_v * x)\mu_B. \tag{2.4}$$

The differences ΔN_v are 4 e^- for the Fe–Ti and 2 e^- in the Mn–V compounds. This results in magnetic moments of 2 μ_B or 1 μ_B at $x = 0.5$. The linear increase with increasing number of valence electrons is clearly seen in Fig. 2.13 for both

series of compounds. The observed deviations—here the higher values in the Ti–Fe compounds at large x—are caused by antisite disorder in the samples. Such disorder is very often observed in Al containing Heusler compounds. The low hybridization strength between Al and the surrounding transition metal atoms allows easily for a swapping between Al and transition metal atoms. The formation of an increase of nearest neighbor transition metals leads in particular for compounds containing Co and Fe to an enhancement of the magnetic moment. From the better agreement of the magnetization of $CoMn_{1+x}V_{1-x}Al$ with the Slater–Pauling values, it is expected that this series is a good candidate for half-metallic ferromagnetism.

In summary, the quaternary Heusler compounds without inversion symmetry $CoFe_{1+x}Ti_{1-x}Al$ and $CoMn_{1+x}V_{1-x}Al$ were synthesized and analyzed by means of X-ray diffraction and magnetometry. The pure compounds ($x = 0$) crystallize in the Y structure with $F\overline{4}3m$ symmetry, due to the 24 valence electrons in the primitive cell they do not carry magnetic moments either in the primitive cell or at the individual sites. This is remarkable—for CoFeTiAl—because CoFe is the transition metal alloy that carries the largest magnetic moment and exhibits the highest known Curie temperature—for CoMnVAl—because Mn carries a localized magnetic moment in all other Heusler compounds. Electronic structure calculations revealed also that the pure compounds do not show magnetic order, in agreement with the experiments. With increasing substitution of Ti by Fe or V by Mn a linear increase of the magnetic moment with the number of valence electrons is observed that agrees with the Slater–Pauling rule, in both experiment and calculations. This demonstrates that the Slater–Pauling behavior of Heusler compounds is not restricted to the $L2_1$ structure with $Fm\overline{3}m$ symmetry but is valid as well in $F\overline{4}3m$ symmetry.

2.8 Transport Properties of Co_2YZ Heusler Compounds

As already mentioned above, the Heusler alloys have attracted a lot of interest as suitable materials for spintronics applications [88] in the recent years. A huge amount of studies investigating the half-metallic properties theoretically and experimentally and enhancing the performance of the compounds and devices for different type of applications were done (see above). The recent observation of the spin Seebeck effect allows to pass a pure spin current over a long distance [89] and is directly applicable to the production of spin voltage generators which are crucial for driving spintronics devices [90–92].

For an effective generation of a spin current the spin Seebeck coefficient and the spin voltage namely the difference in the chemical potential of the spin up $\mu_\uparrow$ and spin down $\mu_\downarrow$ should be large [93]. This section reports on the investigation of Co_2-based Heusler compounds and their potential as spin voltage generators. The high application potential of the compounds is demonstrated. For a further optimization the electronic and magnetic properties of the compounds can be designed easily.

SQUID measurements were carried out to distinguish the saturation magnetization and temperature dependent measurements were done to distinguish the Curie

Table 2.2 Magnetic moments, Curie temperatures, and Seebeck coefficients of the investigated Co_2YZ compounds. The compounds are grouped by their number of valence electrons

Compound	T_c [K]	M_{sat}(5 K) [μ_B]	S(300 K) [μV K^{-1}]
Co_2TiAl	128	0.75	−55
Co_2TiSi	380	1.96	−27
Co_2TiGe	380	1.94	−22
Co_2TiSn	355	1.97	−34
Co_2MnAl	693	3.96	−4
Co_2MnSi	985	4.97	−7
Co_2MnGe	905	4.98	−15
Co_2MnSn	829	5.03	−33
Co_2FeSi	1100	5.97	−12

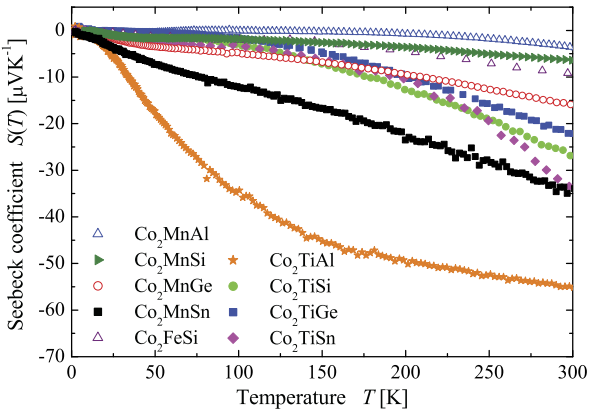

Fig. 2.14 Measured Seebeck coefficients (S) for selected Heusler compounds from 2 K to 300 K

temperatures, the values are summarized in Table 2.2. With the increase of the number of valence electrons and therefore as well the increase of the magnetic moment the Curie temperature increases. One can nicely see the increase of the Curie temperature for the samples with higher numbers of valence electrons. These behavior is well known for Heusler compounds and was reported already some years ago [84, 94]. This measurements show the easy tunability of the magnetic properties of the Heusler compounds. By controlling the number of valence electrons one can design the properties of the materials.

In Fig. 2.14 the measured Seebeck coefficients (S) are displayed for temperatures from 2 K to 300 K. The absolute values increase with increasing temperature. The values at 300 K of all the measurements are summarized in Table 2.2. For an increase of the valence electron count the absolute value of the Seebeck coefficient is decreased. This is explained by the increase of the electron concentration in the bands. By increasing the number of valence electrons additional electrons are added

to the d-band at the Fermi energy [95]. This leads to an increase of the carrier concentration. The increase of the carrier concentration leads to a decrease of the Seebeck coefficient [96]. The interrelationship between carrier concentration and Seebeck coefficient can be seen from relatively simple models of electron transport. For simple metals or degenerate semiconductors with parabolic bands and energy-independent scattering the Seebeck coefficient S is given by

$$S = \frac{8\pi^2 k_B^2}{3eh^2} m^* T \left(\frac{\pi}{3n}\right)^{3/2}, \tag{2.5}$$

where n is the carrier concentration and m^* is the effective mass of the carrier. It can be clearly seen that S depends on the carrier concentration and on the effective mass m^*. The latter depend on the shape of the bands. Although the Seebeck coefficient is decreasing with increasing carrier concentration it is remarkable that Sn containing compounds yield large absolute values for the Seebeck coefficient. This effect is related to changes in the band structure and consequential changes in the effective mass m^*. The Seebeck coefficient of the investigated compounds is negative over the entire temperature range. The found absolute values are quite large compared to elemental metals ($S_{\mathrm{Co}} = -30.8$, $S_{\mathrm{Mn}} = -9.8$, $S_{\mathrm{Ti}} = +9.1$, $S_{\mathrm{Al}} = -1.66$, $S_{\mathrm{Sn}} = -1$, values at $T = 300$ K and in $\mu\mathrm{V\,K^{-1}}$). Especially the Sn containing compounds show high absolute Seebeck coefficients with high Curie temperatures. This makes them attractive candidates for materials used in spin voltage generators.

2.9 Summary

In summary, we reported about the design of materials for spintronics applications. It has been shown that the combination of synthesis and electronic structure calculations is a powerful tool to pick out suitable materials. Starting with $Co_2Cr_{0.6}Fe_{0.4}Al$ and then Co_2FeSi we developed an understanding of the design of new materials and investigated the series $Co_2Mn_{1-x}Fe_xSi$ and $Co_2FeAl_{1-x}Si_x$. From the combination of experimental and theoretical findings (robust gap at $x \approx 0.5 \pm 0.25$) it is concluded that a compound with an intermediate Si concentration close to $x = 0.5 \ldots 0.7$ would be best suited for spintronics applications, especially for GMR and TMR applications. This findings were recently verified by Shan et al. [55] who demonstrated experimentally the half-metallicity of $Co_2FeAl_{0.5}Si_{0.5}$ at room temperature in thin film devices.

In order to separate intrinsic and extrinsic properties, high quality single crystals were grown, especially Co_2FeSi. All Co_2FeSi crystals show excellent ordering, resulting in outstanding electrical behavior with low residual-resistivity and high residual-resistivity-ratio. All Co_2FeSi crystals show constant resistivity below 50 K, which might point to half-metallic ferromagnetism. The cross-over from this unusual to more conventional transport (T^2 dependence) around 50 K indicates the onset of spin flip scattering and thus is indispensable for understanding the strong temperature dependence of Co_2FeSi tunneling magnetoresistance-devices.

Furthermore, it has been shown that synchrotron radiation techniques can solve the problem of crystallographic structure determination, even in the case where the scattering factors of elements in a compound are very similar in response to excitation by traditional lab sources. It is expected that the combination of EXAFS and anomalous XRD may lead to a better understanding of the structure of multilayer thin films in order to improve the quality of TMR-junctions.

As examples of quaternary Heusler compounds without inversion symmetry $CoFe_{1+x}Ti_{1-x}Al$ and $CoMn_{1+x}V_{1-x}Al$ were synthesized and analyzed by means of X-ray diffraction and magnetometry. The pure compounds ($x = 0$) crystallize in the Y structure with $F\overline{4}3m$ symmetry, due to the 24 valence electrons in the primitive cell they do not carry magnetic moments either in the primitive cell or at the individual sites. This is remarkable—for CoFeTiAl—because CoFe is the transition metal alloy that carries the largest magnetic moment and exhibits the highest known Curie temperature—for CoMnVAl—because Mn carries a localized magnetic moment in all other Heusler compounds. Electronic structure calculations revealed also that the pure compounds do not show magnetic order, in agreement with the experiments. With increasing substitution of Ti by Fe or V by Mn a linear increase of the magnetic moment with the number of valence electrons is observed that agrees with the Slater–Pauling rule, in both experiment and calculations. This demonstrates that the Slater–Pauling behavior of Heusler compounds is not restricted to the $L2_1$ structure with $Fm\overline{3}m$ symmetry but is valid as well in $F\overline{4}3m$ symmetry.

In the last section, Co_2-based Heusler compounds have been investigated on their potential use as spin voltage generators. The observed Seebeck coefficients were all negative in the whole temperature range. The absolute values are quite large compared to simple metals. Especially the Sn containing compounds show high Seebeck coefficients with high Curie temperatures. This makes them attractive candidates for materials used in spin voltage generators.

Acknowledgements This work was financially supported by the Deutsche Forschungsgemeinschaft (project P 1 in DfG research unit FOR 559). Additional financial support by the DAAD (D06/33952), CAPES PROBRAL (167/04), and Stiftung Innovation Rheinland-Pfalz is gratefully acknowledged. The authors thank Y. Hwu (Taipei, Taiwan), K. Kobayashi (Hyogo, Japan), H.-J. Lin (Hsinchu, Taiwan), J. Morais, M.C.M. Alves, F. Bernardi, (Porto Alegre, Brazil), R. Seshadri (Santa Barbara, USA) as well as V. Alijani, J. Barth, L. Basit, S. Berinskat, C.G.F. Blum, F. Caspar, T. Gasi, T. Graf, V. Jung, H.C. Kandpal, V. Ksenofontov, S. Ouardi, W. Tremel, J. Winterlik, and S. Wurmehl and all the student assistants during the last six years for their help with theory and experiments, and for fruitful discussions. Assistance by the staff of the synchrotron facilities BESSY (Berlin, Germany), LNLS (Campinas, Brazil), NSRRC (Hsinchu, Taiwan) and SPRING-8 (Hyogo, Japan) is gratefully acknowledged.

References

1. Prinz GA (1998) Science 282:1660
2. de Groot RA, Müller FM, Engen PGv, Buschow KHJ (1983) Phys Rev Lett 50:2024
3. Coey JMD, Venkatesan M, Bari MA (eds) (2002) Half-metallic ferromagnets. Lecture notes in physics, vol 595. Springer, Heidelberg

4. Youn SJ, Min BI (1995) Phys Rev B 51:10436
5. Ristoiu D, Nozieres JP, Borca CN, Borca B, Dowben PA (2000) Appl Phys Lett 76:2349
6. Ristoiu D, Nozieres JP, Borca CN, Komesu T, Jeong HK, Dowben PA (2000) Europhys Lett 49:624
7. Zhu W, Sinkovic B, Vescovo E, Tanaka C, Moodera JS (2001) Phys Rev B 64:R060403
8. Kübler J, Williams AR, Sommers CB (1983) Phys Rev B 28:1745
9. Webster PJ, Ziebeck KRA (1973) J Phys Chem Solids 34:1647
10. Heusler F (1903) Verh Dtsch Phys Ges 5:219
11. Block T, Felser C, Jakob G, Ensling J, Mühling B, Gütlich P, Beaumont V, Studer F, Cava RJ (2003) J Solid State Chem 176:646
12. Block T, Wurmehl S, Felser C, Windeln J (2006) Appl Phys Lett 88:202504
13. Inomata K, Okamura S, Goto R, Yezuka N (2003) Jpn J Appl Phys 42:L419
14. Kelekar R, Clemens BM (2004) J Appl Phys 96:540
15. Hirohata A, Kikuchi M, Tezuka N, Inomata K, Claydon JS, Xu YB (2005) J Appl Phys 97:10C308
16. Hirohata A, Kurebayashi H, Okamura S, Kikuchi M, Masaki T, Nozaki T, Tezuka N, Inomata K (2005) J Appl Phys 97:103714
17. Jakob G, Casper F, Beaumont V, Falka S, Auth N, Elmers HJ, Felser C, Adrian H (2005) J Magn Magn Mater 290–291:1104
18. Inomata K, Tezuka N, Okamura S, Kurebayashi H, Hirohata A (2004) J Appl Phys 95:7234
19. Marukame T, Kasahara T, Matsuda KI, Uemura T, Yamamoto M (2005) Jpn J Appl Phys 44:L521
20. Auth N, Jakob G, Block T, Felser C (2003) Phys Rev B 62:024403
21. Conca A, Falk S, Jakob G, Jourdan M, Adrian H (2005) J Magn Magn Mater 290–291:1127
22. Clifford E, Venkatesan M, Gunning R, Coey JMD (2004) Solid State Commun 131:61
23. Rodrìgues-Carval J (1993) Physica B 55:192
24. Ferreira FF, Granado E, Carvalho W Jr., Kycia SW, Bruno D, Droppa R Jr. (2006) J Synchrotron Radiat 13:46
25. Wurmehl S, Fecher GH, Kandpal HC, Ksenofontov V, Felser C, Lin HJ, Morais J (2005) Phys Rev B 72:184434
26. Ouardi S, Gloskovskii A, Balke B, Jenkins CA, Barth J, Fecher GH, Felser C, Gorgoi M, Mertin M, Schäfers F, Ikenaga E, Yang K, Kobayashi K, Kubota T, Oogane M, Ando Y (2009) J Phys D, Appl Phys 42:084011
27. Graf T, Fecher GH, Barth J, Winterlik J, Felser C (2009) J Phys D, Appl Phys 42:084003
28. Barth J, Fecher GH, Balke B, Ouardi S, Graf T, Felser C, Shkabko A, Weidenkaff A, Klaer P, Elermers HJ, Yoshikawa H, Ueda S, Kobayashi K (2010) Phys Rev B 81:064404
29. Wurmehl S, Alves MCM, Morais J, Ksenofontov V, Teixeira SR, Machado G, Fecher GH, Felser C (2007) J Phys D, Appl Phys 40:1524
30. Wurmehl S, Fecher GH, Kandpal HC, Ksenofontov V, Felser C, Lin HJ (2006) Appl Phys Lett 88:032503
31. Wurmehl S, Morais J, Alves MdCM, Teixeira SR, Fecher GH, Felser C (2006) J Alloys Compd 423:159
32. Wurmehl S, Fecher GH, Felser C (2006) Z Naturforsch 61b:749
33. Wurmehl S, Fecher GH, Kroth K, Kronast F, Dürr HA, Takeda Y, Saitoh Y, Kobayashi K, Lin HJ, Schönhense G, Felser C (2006) J Phys D, Appl Phys 39:803
34. Wurmehl S, Fecher GH, Ksenofontov V, Casper F, Stumm U, Felser C, Lin HJ, Hwu Y (2006) J Appl Phys 99:08J103
35. Fuji S, Sugimura S, Ishida S, Asano S (1990) J Phys Condens Matter 2:8583
36. Brown PJ, Neumann KU, Webster PJ, Ziebeck KRA (2000) J Phys Condens Matter 12:1827
37. Ravel B, Raphael MP, Harris VG, Huang Q (2002) Phys Rev B 65:184431
38. Geiersbach U, Bergmann A, Westerholt K (2002) J Magn Magn Mater 240:546
39. Kämmerer S, Heitmann S, Meyners D, Sudfeld D, Thomas A, Hütten A, Reiss G (2003) J Appl Phys 93:7945

40. Singh LJ, Barber ZH, Miyoshi Y, Bugoslavsky Y, Branford WR, Cohen LF (2004) Appl Phys Lett 84:2367
41. Wang WH, Przybylski M, Kuch W, Chelaru LI, Wang J, Lu F, Barthel J, Meyerheim HL, Kirschner J (2005) Phys Rev B 71:144416
42. Wang WH, Przybylskia M, Kuch W, Chelaru LI, Wang J, Lu YF, Barthel J, Kirschner J (2005) J Magn Magn Mater 286:336
43. Schmalhorst J, Kämmerer S, Sacher M, Reiss G, Hütten A, Scholl A (2004) Phys Rev B 70:024426
44. Schmalhorst J, Kammerer S, Reiss G, Hütten A (2005) Appl Phys Lett 86:052501
45. LeClair P, Swagten HJM, Kohlhepp JT, de Jonge WJM (2000) Appl Phys Lett 76:3783
46. Kandpal HC, Fecher GH, Felser C, Schönhense G (2006) Phys Rev B 73:094422
47. Balke B, Fecher GH, Kandpal HC, Felser C, Kobayashi K, Ikenaga E, Kim JJ, Ueda S (2006) Phys Rev B 74:104405
48. Inomata K, Okamura S, Miyazaki A, Kikuchi M, Tezuka N, Wojcik M, Jedryka E (2006) J Phys D, Appl Phys 39:816
49. Oogane M, Sakuraba Y, Nakata J, Kubota H, Ando Y, Sakuma A, Miyazaki T (2006) J Phys D, Appl Phys 39:834
50. Ebke D, Schmalhorst J, Liu NN, Thomas A, Reiss G, Hütten A (2006) Appl Phys Lett 89:162506
51. Tezuka N, Ikeda N, Miyazaki A, Sugimoto S, Kikuchi M, Inomata K (2006) Appl Phys Lett 89:112514
52. Tezuka N, Ikeda N, Sugimoto S, Inomata K (2006) Appl Phys Lett 89:252508
53. Fecher GH, Felser C (2007) J Phys D, Appl Phys 40:1582
54. Kobayashi K, Umetsu RY, Kainuma R, Ishida K, Oyamada T, Fujita A, Fukamichi K (2004) Appl Phys Lett 85:4684
55. Shan R, Sukegawa H, Wang WH, Kodzuka M, Furubayashi T, Ohkubo T, Mitani S, Inomata K, Hono K (2009) Phys Rev Lett 102:246601
56. Furubayashi T, Kodama K, Nakatani TM, Sukegawa H, Takahashi YK, Inomata K, Hono K (2010) J Appl Phys 107:113917
57. Kübler J, Fecher GH, Felser C (2007) Phys Rev B 76:024414
58. Galanakis I, Dederichs PH (eds) (2005) Half-metallic alloys. Lecture notes in physics, vol 676. Springer, Berlin
59. Ravel B, Cross JO, Raphael MP, Harris VG, Ramesh R, Saraf V (2002) Appl Phys Lett 81:2812
60. Tampo H, Fons P, Yamada A, Kim KK, Shibata H, Matsubara K, Niki S, Yoshikawa H, Kanie H (2005) Appl Phys Lett 87:141904
61. Zhu Q, Li L, Masteller MS, Corso GJD (1996) Appl Phys Lett 69:3917
62. Chow GM, Sun CJ, Soo EW, Wang JP, Lee HH, Noh DY, Cho TS, Je JH, Hwu YK (2002) Appl Phys Lett 80:1607
63. Cross JO, Newville M, Rehr JJ, Sorensen LB, Bouldin CE, Watson G, Gouder T, Lander GH, Bell MI (1998) Phys Rev B 58:11215
64. Graf T, Casper F, Winterlik J, Balke B, Fecher GH, Felser C, Anorg Z (2009) Z Anorg Allg Chem 635:976
65. Gercsi Z, Rajanikanth A, Takahashi YK, Hono K, Kikuchi M, Tezuka N, Inomata K (2006) Appl Phys Lett 89:082512
66. Ishikawa T, Marukame T, Kijima H, Matsuda Ki, Uemura T, Yamamoto M (2006) Appl Phys Lett 89:192505
67. Tsunegi S, Sakuraba Y, Oogane M, Takanashi K, Ando Y (2008) Appl Phys Lett 93:112506
68. Oogane M, Shinano M, Sakuraba Y, Ando Y (2009) J Appl Phys 105:07C903
69. Chioncel L, Sakuraba Y, Arrigoni E, Katsnelson MI, Oogane M, Ando Y, Miyazaki T, Burzo E, Lichtenstein AI (2008) Phys Rev Lett 100:086402
70. Ambrose T, Krebs JJ, Prinz GA (2000) Appl Phys Lett 76:3280
71. Raphael MP, Ravel B, Willard MA, Cheng SF, Das BN, Stroud RM, Bussmann KM, Claassen JH, Harris VG (2001) Appl Phys Lett 79:4396

72. Schneider H, Jakob G, Kallmayer M, Elmers HJ, Cinchetti M, Balke B, Wurmehl S, Felser C, Aeschlimann M, Adrian H (2006) Phys Rev B 74:174426
73. Paudel MR, Wolfe CS, Patton HMA, Simonson J, Dubenko I, Ali N, Stadler S (2009) J Appl Phys 105:07E902
74. Otto MJ, van Woerden RAM, van der Valk PJ, Wijngaard J, van Bruggen CF, Haas C (1989) J Phys Condens Matter 1:2351
75. Schmalhorst J, Ebke D, Weddemann A, Hütten A, Thomas A, Reiss G, Turchanin A, Gölzhäuser A, Balke B, Felser C (2008) J Appl Phys 104:043918
76. Inomata K, Ikeda N, Tezuka N, Goto R, Sugimoto S, Wojcik M, Jedryka E (2008) Sci Technol Adv Mater 9:014101
77. Blum CGF, Jenkins CA, Barth J, Felser C, Wurmehl S, Friemel G, Hess C, Behr G, Büchner B, Reller A, Riegg S, Ebbinghaus SG, Ellis T, Jacobs PJ, Kohlhepp JT, Swagten HJM (2009) Appl Phys Lett 95:161903
78. Matsuda K, Hiroi M, Kawakami M (2005) J Phys Condens Matter 17:5889
79. Kusakari Y, Kanomata T, Fukushima K, Nishihara H (2007) J Magn Magn Mater 310:e607
80. Picozzi S, Continenza A, Freeman AJ (2002) Phys Rev B 66:094421
81. Galanakis I, Dederichs PH, Papanikolaou N (2002) Phys Rev B 66:174429
82. Pugacheva M, Jezierski A (1995) J Magn Magn Mater 151:202
83. Klaer P, Kallmayer M, Elmers HJ, Basit L, Thöne J, Chadov S, Felser C (2009) J Phys D, Appl Phys 42:084001
84. Fecher GH, Kandpal HC, Wurmehl S, Felser C, Schönhense G (2006) J Appl Phys 99:08J106
85. Kübler J (2000) Theory of itinerant electron magnetism. Oxford University Press, Oxford
86. Wurmehl S, Kandpal HC, Fecher GH, Felser C (2006) J Phys Condens Matter 18:6171
87. Pickett WE (1998) Phys Rev B 57:10613
88. Felser C, Fecher GH, Balke B (2007) Angew Chem, Int Ed 46:668
89. Uchida K, Takahashi S, Harii K, Ieda J, Koshibae W, Ando K, Maekawa S, Saitoh E (2008) Nature 455:778
90. Wolf SA, Awschalom DD, Buhrman RA, Daughton JM, von Molnar S, Roukes ML, Chtchelkanova AY, Treger DM (2001) Science 294:1488
91. Zutic I, Fabian J, Sarma SD (2004) Rev Mod Phys 76:323
92. Chappert C, Fert A, Van Dau FN (2007) Nat Mater 6:813
93. Ong NP (2008) Nature 455:741
94. Kandpal HC, Felser C, Fecher GH (2007) J Magn Magn Mater 310:1626
95. Ouardi S, Balke B, Gloskovskii A, Fecher GH, Felser C, Schönhense G, Ishikawa T, Uemura T, Yamamoto M, Sukegawa H, Wang W, Inomata K, Yamashita Y, Yoshikawa H, Ueda S, Kobayashi K (2009) J Phys D, Appl Phys 42:084010
96. Snyder GJ, Toberer ES (2008) Nat Mater 7:107

http://www.springer.com/978-90-481-3831-9

Spintronics
From Materials to Devices
Felser, C.; Fecher, G.H. (Eds.)
2013, XXI, 369 p., Hardcover
ISBN: 978-90-481-3831-9